Contents lists available http://www.kinnaird.edu.pk/

Journal of Natural and Applied Sciences Pakistan

Journal homepage: http://jnasp.kinnaird.edu.pk/

SYNTHESIS OF MANGANESE-COBALT HYDROUS OXIDES NANOPARTICLES DOPED BIOCHAR FOR REMOVAL OF CHROMIUM (VI) FROM WATER

Sana Khalid[1]*, Rabia Nazir[2], Sajid Rashid Ahmad[1], Muhammad Nawaz Chaudhry[3], Muhammad Ibrar[4], Fahad Ali[5]

[1] University of the Punjab, Lahore, Pakistan

[2] Pakistan Council of Scientific and Industrial Research Laboratories Complex, Ferozepur Road, Lahore, Pakistan

[3] Lahore School of Economics (LSE), Lahore, Pakistan

[4] Lahore Garrison University, Lahore, Pakistan

[5] Department of Chemistry, Government Postgraduate College, Gujranwala, Pakistan

Article Info

*Corresponding Author
Email: sanakhalid305@gmail.com

Abstract

Water is an inherent medium required for survival of living organisms. Treatment of wastewater loaded with toxic metals to make it suitable for consumption, is one of the massive challenges being faced globally. Nano-adsorption has served as an advanced and compelling approach toward decontamination of environmental contaminants from water. Over the past few decades, biochar and biochar based composites have emerged as extraordinary adsorbents with highly efficient, affordable and environment friendly properties for sequestration of hazardous metals from aqueous environment. In this study, the adsorption of Cr(VI) ions from aqueous solution was examined using manganese-cobalt hydrous oxides nanoparticles decorated biochar (MRHBC) by batch adsorption technique and the impact of different adsorption parameters, such as contact time, temperature, solution pH, adsorbent dosage and initial metal ion concentration were investigated. The MRHBC was characterized by FTIR, SEM-EDX and XRD. The MRHBC was effective for the maximum uptake (95%) of Cr(VI) at pH 3.0, and equilibrium was achieved in 60 min. The adsorption data was fitted to various kinetic models and adsorption isotherms. Fitting of experimental data to these models exhibited best-fit models to be the general-order kinetic model and Langmuir adsorption model for removal of Cr(VI) ions from aqueous solution. The maximum uptake capacity of biochar composite with respect to Cr(VI) ions calculated from Langmuir isotherm was found to be 232.75 mg g^{-1}.

Keywords
Biochar; Manganese-Cobalt Hydrous Oxide Nanoparticles; Chromium; Kinetic Models; Adsorption Isotherms; Water Treatment

The global scarcity in freshwater reserves, poor quality and inequitable distribution of water supplies have urged the exigency to preserve existing water resources for sustainable growth (Mosa *et al*., 2016). The recent advancement in industrialization and urbanization have exerted collateral pressure on freshwater supplies with the unchecked release of wastewater containing several types of pollutants into aquatic environment (Garcia & Pargament, 2015). Heavy metal pollution is a global burning issue causing massive environmental impairment and potential health hazards to all life forms since these are highly toxic, persistent, non-biodegradable, and may bio-accumulate and bio-concentrate in ecosystem once entered into the food chain (Xiao, Wang, Li, Wang, & Zhang, 2017). Chromium, a highly hazardous metals, has wide applications in multiple industrial sectors including electroplating, ceramics, textile dyeing and printing, wood processing and lather tanning etc. (Katz & Salem, 1994; Polowczyk, Urbano, Rivas, Bryjak, & Kabay, 2016). It occurs in aquatic systems in two oxidation forms i.e., trivalent (Cr (III)) and hexavalent (Cr (VI)) and is highly mobile in aqueous environment as compared to Cr (III), making it 1000 folds more toxic and mutagenic (Mishra & Bharagava, 2016; Qiao *et al*., 2020). It is known to induce several health issues including lungs cancer, liver and kidneys disorders, skin disease and genetic alterations (Nickens, Patierno, & Ceryak, 2010) hence, it is enlisted as priority contaminant by US Environmental Protection Agency (EPA) (Costa, 2003). Thus, the acute toxicity of Cr(VI) has urged the requirement for its effective removal from environment. Decontamination of heavy metals from wastewater is a highly challenging task. Vast numbers of water purification technologies including ion exchange, membrane filtration, chemical precipitation, electro-dialysis, biodegradation, and adsorption have been explored for heavy metals removal from wastewater (Abyaneh & Fazaelipoor, 2016; Fraser, Pritzker, & Legge, 1994; Habiba *et al*., 2017; Kaya, Onac, & Alpoguz, 2016; Korak, Huggins, & Arias-Paic, 2017; Qhubu, Methula, Xaba, Moyo, & Pakade, 2021). Though, adsorption is suggested highly convenient and compelling approach for heavy metals abatement in terms of operational convenience and environmental-friendliness. In recent times, a great attention has been given to the use of agroforestry wastes based adsorbents for wastewater treatment because of the ease of availability, environment-friendly nature and low economic cost (Khalil *et al.,* 2020; Mohamed & Mahmoud, 2020; Qhubu *et al*., 2021; S. Xu *et al.*, 2021). Bulk quantities of rice husk are generated as an agricultural waste biomass during rice processing, which are often indiscriminately discarded as solid waste, causing severe environmental pollution. During (2012-2015), the average yield of rice husk was accounted 1828 tons/year in Pakistan (Mirani, Kalwar, & Ahmad, 2013). Thereof, converting the rice husk into biochar for sequestration of heavy metals could be a viable approach for environmental

remediation. Biochar has been emerged as a superior adsorbent for the removal of heavy metals from wastewater (Mohadi *et al*., 2021). However, most of the pristine biochar exhibit lower adsorption potential than modified biochar based adsorbents. Furthermore, the integration of metal nanoparticles of interest has also been suggested to augment the specific surface area and surface reactive groups, resulting in profound uptake of heavy metals (Zhu, Huang, Wang, Wang, & Ma, 2018). There is great line of evidences showing the effective potential of metal/metal oxide-biochar based composites for heavy metals sequestration (Table 1). Cobalt doped bamboo biochar was found capable of removing Cr (VI) with an adsorption capacity of 45.45 mg g-1 (Y. Wang *et al*., 2012). Zinc chloride modified cassava sludge biochar removed 8.44 mg of Cr (VI)/g of adsorbent (J. Yang, Li, Yang, Kang, & Zhang, 2018). Effective adsorption of Cr(VI) was also reported by using Fe-Mn oxide decorated aquatic reed biochar under acidic pH (3.0), achieving maximum adsorption capacity of 59.81 mg g-1 (B. Wang, Li, Wang, & Ecology, 2020). Zhang *et al*. reported the superior uptake efficiency of N-Fe co-impregnated oak wood biochar, enabling removal of Cr (VI) up to 99.9% within 10 minutes at adsorbent dose of 1g L-1 and Cr (VI) baseline concentration of 50 mg L-1 (Y. Zhang *et al*., 2020). Therefore, by considering the plausibility of biochar and nanomaterials toward viable decontamination of heavy metals from aqueous environment, the current study for the very first time has directed at fabrication and application of rice husk derived biochar anchored metal nanocomposite for treatment of Cr (VI) polluted water.

2. Experimental Section

All the chemicals used in this study were of analytical grade purity. The solutions were prepared in distilled water. Manganese sulphate monohydrate, potassium dichromate, sodium hydroxide and nitric acid were purchased from Sigma Aldrich, and cobalt chloride hexahydrate was obtained from Daejung Chemicals. Hydrochloric acid was procured from Pakistan Council of Scientific and Industrial Research (PCSIR) Lahore, Pakistan. All the chemicals were used as received without further purification.

2.1.Synthesis of Hydrous Metal Oxides Nanoparticles Doped Biochar

Rice husk, collected from a local rice mill located in Lahore, Pakistan, was washed thoroughly with distilled water to remove dirt and impurities and allowed to air dry for 24 hours. The dried rice husk was pulverized into fine powder and passed through 250micron sieve. Subsequently, it was pyrolysed at 500oC for 2 hours in limited supply of oxygen to produce biochar. For activation, the prepared biochar was reacted with 2% sulphuric acid under constant heating and agitation for 1 hour. The resultant solution mixture was cooled down, residues were filtered and washed with distilled water until its pH became neutral. 50 g of acid activated biochar was then dispersed in 1L distilled water and the mixture was allowed to stir

until homogeneously distributed. To this suspension, 100 ml of 0.05 M cobalt chloride and manganese sulphate solutions prepared were added dropwise under vigorous agitation, followed by dropwise inclusion of 200 ml of sodium hydroxide (1M) to form precipitates of composite. The resultant suspension was filtered, residue was washed with distilled water and oven dried at 110oC for overnight. The as fabricated biochar composite was ground, stored in air tight container and denoted as MRHBC. The Fig. 1 presents the schematic illustration of stepwise fabrication of MRHBC.

2.2.Characterization of Metal Doped Biochar

Scanning electron microscopy and Energy Dispersive X-ray (SEM-EDX) analysis were employed by using Nova NanoSEM 450 field-emission scanning electron microscope (FE-SEM) to examine the surface morphology and chemical composition of MRHBC. Fourier transform infrared spectroscopy (FTIR) was carried out using Tensor-27 for determining the surface functional groups of fabricated biochar composite. The crystalline nature and phase of sample was examined by using X-ray Diffractometer (Bruker, D2-Phaser).

2.3. Adsorption Studies

Batch experiments were carried out to investigate the adsorption of Cr(VI) onto MRHBC under varying conditions of different experimental parameters (i.e., contact time, temperature, solution pH, adsorbent dose and initial metal ion concentration). To perform this stock solution of Cr(VI) (1000 mg L-1) was prepared by dissolving 2.83 g of potassium dichromate (K2Cr2O7) salt in 500 ml distilled water and making the final volume up to 1000 ml. The working solutions of preferred concentrations were made by diluting the stock solution. For a series of experiments to be carried out to optimize the process parameters required for maximum metal adsorption, 50 ml of known concentration of Cr(VI) ion solution (300-1000 mg L-1) taken in a conical flask with known dose of adsorbent (0.025-0.5 g) was stirred at 200 rpm for a given time period (10-90 min) at constant temperature (20-80oC). The pH (1.0-8.0) of the solution was adjusted with the help of 0.1M HCl and 0.1 M NaOH. Afterwards, the sample suspension was filtered using filter paper (Whatmann No. 42, ashless) to separate out solid and liquid phases. The residual amount of Cr(VI) in filtrate was analyzed with the help of flame atomic absorption spectrometer (PerkinElmer AAnalyst 200). The percentage removal efficiency (RE%) and the concentration of adsorbate sorbed on adsorbent (Adsorption capacity (mg g-1), qexp) were calculated using Equation (1) and (2).

$$RE\ (\%)=[(C_i-C_f)/C_i\ ]\times 100 \quad (1)$$

$$q_{exp}=(C_i-C_f\ )\times V/W \quad (2)$$

where, Ci (mg L-1) and Cf (mg L-1) are the initial and final concentration of adsorbate in solution, respectively, V (L) is the volume of solution and W (g) is the mass of adsorbent.

3. Results and Discussion

3.1. Synthesis of Hydrous Metal Oxides Nanoparticles Doped Biochar

The nanocomposite was synthesized using rice husk biochar as support. Rice husk constitutes approximately 50% cellulose, 25–30% lignin, 15–20 % silica, and 10–15% moisture content. It offers a suitable carbon precursor due to its high lignocellulose content. Biochar was fabricated by slow pyrolysis (500oC) of rice husk in oxygen deficit environment and volatilization of lignocellulosic content of biomass during carbonization promoted the development of porous structure in biochar. Manganese/Cobalt hydrous oxide nanoparticles were incorporated into the porous structure of the biochar by using simple chemical precipitation method. The prepared biochar was characterized using different techniques and checked for its efficacy as potential adsorbent for removal of Cr(VI), a potential contaminant of leather industry waste.

3.2. Characterization of Hydrous Metal Oxides Nanoparticles Doped Biochar

3.2.1. FTIR

The FT-IR spectra of MRHBC is presented in Fig. 2a. The–OH groups due to adsorbed moisture in the sample generated weak signals in the spectra at 3360 cm−1 (Aguilar, García, Soto-Garrido, & Arriagada, 2003). The peaks evidenced at 2320, 2095 and 2000 cm−1 are attributed to C ≡ C stretching; the band at 1575 cm−1 is related to –COO stretching vibrations (Kamran & Park, 2020). The -CH2 or -CH3 bending vibrations were detected at 1375 cm-1 (Liu, Li, & Singh, 2021). The strong signal at 1035 cm−1 corresponds to C–O stretching and C–OH bending (Kamran & Park, 2020; Liu *et al*., 2021), while the peak at 794 cm−1 refers to asymmetrical bending vibration of Si–O–Si bond (Mohan *et al*., 2018).

3.2.2. SEM-EDX

SEM-EDX analysis were performed for investigating surface morphology and elemental composition of the biochar nanocomposite matrix. SEM micrograph along with EDX mapping of MRHBC is shown in Fig. 2b and 2c. Fig. 2b displays typical framework of biochar presenting lamellar layering of porous biochar with homogeneous distribution of manganese hydroxide (Mn(OH)2) and cobalt hydroxide (Co(OH)2) nanoparticles deposited on its surface. The inset image of MRHBC exhibits that manganese and cobalt hydroxide nanoparticles possess fluffy texture, occurring in agglomerated form above the surface of biochar. These findings are in agreement with the earlier studies (Kamran & Park, 2020). EDX spectrum is presented in Fig. 2c, which summarizes the percentage (%) weight of the major elemental components of MRHBC. C peak is highly prominent in the spectrum, with the % weight of 68.64% owing to the biochar while Si accounts 3.41 % weight ratio, which is a chief constituent of rice husk. The quantitative data confirms the presence of Mn (0.94%) and Co (0.81%) metals in the composite. Other elements like Na, K, are probably presenting due to the presence in rice husk biomass.

3.2.3. XRD

Fig. 2d represents the powder XRD diffractogram of MRHBC. The peak plane hkl (002) corresponds to carbon (C); the broadening of which ascribes the amorphous structure of biochar (T. Chen, Liu, & Scott, 2016). The sharp peak with crystal plane index (110) refers to crystalline silica (quartz), which matches well with JCPDS card no. 46-1045 (Mohan *et al*., 2018; X. Xu, Hu, Ding, & Chen, 2017). The diffraction peak planes corresponding to hkl values of (011), (012), (110) and (201) are indexed to Mn(OH)2, which is in good agreement with JCPDS card no. 73-1604 (X. Zhang, Qian, Zhu, & Tang, 2014), while peaks referring to planes values of (101), (002), (110) and (103) conform to the Co(OH)2 (JCPDS card no. 45-0031) (Shokrani-Havigh & Azizian-Kalandaragh, 2017; Zhou *et al*., 2022). The low peak intensity of metal hydroxides corresponds to their poor crystalline nature and smaller crystallite size indicating formation of nanocomposite (Kamran & Park, 2020).

3.3. Adsorption Studies

The prepared nanocomposite was checked for its efficacy against Cr(VI) removal from aqueous media in batch mode as function of varying experimental conditions (contact time, temperature, solution pH, adsorbent dose and initial metal ion concentration).

3.3.1. Effect of contact time and Adsorption Kinetics

Contact time is an imperative parameter to be studied during the adsorption experiments (Khalil *et al*., 2020). The impact of variation of contact time on adsorption of Cr(VI) onto MRHBC is represented in Fig. 3a. The influence of contact time on the adsorption of Cr(VI) by adsorbent was investigated by agitating 50ml of Cr(VI) ion solution (500 mg L-1) in 250 ml conical flask with 0.1 g of adsorbent at room temperature and initial solution pH 4.0 for varied time intervals ranging 10-90 minutes. In the beginning the sorption process was very rapid due to bulk density of active sites on the adsorbents' surface being available for binding with metal ions, leading to fast reaction rate. The Cr(VI) ions uptake on MRHBC increased with increase in contact time until equilibrium phase was achieved at 80 minutes. As the adsorption process proceeded, the decrease in number of vacant sites occurred because these were occupied by metal ions, leading to decrease in metal adsorption. In a study, for adsorption of Cr(VI) from aqueous media onto acid activated corn cob biochar, Murugesan *et al*. investigated the 60 min of contact time for maximum removal (Murugesan *et al*., 2013). Sarkar *et al*. determined the removal of Cr(VI) on sulfuric acid modified rice husk biochar and reported 120 min as the optimized contact time (Sarkar, Ranjan, Paul, & Policy, 2019). Adsorption kinetics delineates the sorption rate of solute onto the adsorbent and is very salient function to evaluate the removal efficiency of an adsorbent. Different kinetics models (Pseudo-first-order (Lin & Wang, 2009), Pseudo-second-order (Boparai, Joseph, & O'Carroll, 2011), general-order (Saucier *et al*., 2015) and Elovich (Ho & McKay, 2002)) in non-

linear form mentioned in equation (3-6), respectively, were fitted to experimental data (Fig. 3b).

$$q_t = q_e[1 - exp(-k_1 \cdot t)] \quad (3)$$

$$q_t = \frac{t \cdot k_2 \cdot q_e^2}{1 + t \cdot k_2 \cdot q_e} \quad (4)$$

$$q_{t} = q_e - \frac{q_e}{\left[k_3 \cdot \left(q_e{}^{(n-1)}\right) \cdot t \cdot (n-1) + 1\right]^{(1/1-n)}} \quad (5)$$

$$q_t = \frac{1}{b}\,[ln\,(a \cdot b \cdot t + 1)] \quad (6)$$

Where, qt (mg g-1) is the concentration of adsorbent at time t (min), qe (mg g-1) is the concentration at equilibrium, k1 (min-1) and k2 (g mg-1 min-1) and k3 (min−1 (g mg−1) n−1) are the rate constants for pseudo-first, pseudo-second and general orders, respectively, a (mg g-1 min-1) is the initial rate of adsorption, b (g mg-1) is the desorption constant and n is the kinetic sorption order (n could be an integer or a fractional value). The best fitting of model was assumed from highest R2, lowest reduced chi-square and standard deviation values, and smallest difference between experimental (qe,exp) and calculated (qe,cal) adsorption capacity. The adoption data did not fit to pseudo-first-order kinetic model (data not shown), while other three models registered good-fitting to the experimental data. The adsorption process followed general order kinetics model as justified by higher R2 (0.99725), and qe,exp (127.81 mg g-1) is closely near to qe,cal (133.79 mg g-1). The kinetic modelling parameters are given in Table (2).

3.3.2. Effect of Temperature

To investigate the effect of temperature, a set of experiments were performed by varying temperature from 20-80oC, while keeping the other parameters (contact time (60 min), pH (4.0), adsorbent dose (0.1 g) and Cr(VI) ion concentration (50ml of 500 mg L-1)) fixed. The Fig. 4a represents the impact of temperature variation on the removal of Cr(VI) onto MRHBC from aqueous media. The % metal adsorption efficiency enhances with increase in temperature because of thermal activation of metal ions which results in increased movements of metal ions, thereby leading to high adsorption (Guo, Lv, Yang, Xu, & Song, 2021; M.-m. Zhang *et al*., 2015). The metal adsorption augmented incrementally with increase in temperature up to 50oC. However, further temperature increase from 60 to 80oC registered insignificant increase in adsorption since equilibrium point was achieved. Moreover, the desorption of adsorbed metal species may occur at high temperatures

which lowers the adsorption activity and points to easy desorption of the prepared adsorbent.

3.3.3. Effect of pH

The pH of solution is an important experimental parameter, which is highly necessary to be considered in adsorption studies as it controls the binding of metal ions onto the adsorbent surface. In order to determine the effect of pH on Cr(VI) ion adsorption, experiments (batch mode) were conducted at different pH values ranging from 1.0 to 8.0 and studies at pH >8.0 were not performed due to formation of metal precipitates. The pH of the solution was adjusted with the help of 0.1 M HCL and 0.1 M NaOH. For this, 50 ml of Cr(VI) solution (500mg L-1) was contacted for 60 minutes with 0.1 g of adsorbent at temperature (50oC) and altering pH levels (1.0-8.0). In acidic medium, hydrogen chromate (HCrO4-) ions are the most predominant form of Cr(VI); and when the pH moves towards basic medium the chromate ions (CrO42-) are the most prevalent specie to occur in the aqueous system (X. S. Wang *et al*., 2010). The Fig. 4b represents the influence of pH variation on the removal of Cr(VI) onto MRHBC from aqueous media. The % removal of Cr(VI) augments with decrease in pH (acidic) and the maximum adsorption of Cr(VI) (69.8%) was recorded at pH 3.0. At low pH, the adsorbent surface becomes protonated due to presence of excessive H+ ions in the aqueous solution which facilitates the binding of Cr(VI) as HCrO4-. When the pH is enhanced, the degree of protonation lowers gradually due to increase in number of OH- ions and the biochar surface gets anionic charge which results in electrostatic repulsion between negatively charged adsorbents' surface and Cr(VI) ionic species, leading to poor metal uptake activity (Shang, Zhang, Jin, & Gao, 2014). The similar response was evidenced in the present study in which high adsorption of Cr(VI) ions onto the fabricated composite was noticed in acidic medium (pH 3.0) and began to decreased when the pH shifted to neutral or alkaline medium.

3.3.4. Effect of Adsorbent Dose

The impact of adsorbent dose on Cr(VI) uptake was studied (in batch mode) by varying its dose (0.025-0.5g) at optimized time (60 min), pH (3.0), temperature (50oC) and using 500 mg L-1 of metal ion solution. It can be seen from the graph (Fig. 4c) that with the increase in adsorbent dosage from 0.025 to 0.1 g, there is a conspicuous increase in % removal efficiency (8.8 – 69.6%) of Cr(VI) by MRHBC, followed by a relatively slow increase in % adsorption efficiency (74.7-89.8%) when adsorbent dose was increased from 0.15-0.5g (Fig. 4c). This increase in % removal efficiency of Cr(VI) is attributed to increase in the binding sites and surface functional groups for adsorption of metal ions. The maximum adsorption capacity was observed at 0.1 g dose, so it is regarded as optimum dosage for sorption activity. However, for increase in adsorbent dose above the 0.1 g, the significant decrease in adsorption capacity was observed. This is attributed to the fact that increase in adsorbent dose increases the number of binding sites which initially encourages the uptake potential, but the

sorption capacity compromised beyond the optimum dose as vast number of binding sites are left unsaturated since adsorbent dose is increased at constant concentration of adsorbate (Khalil *et al*., 2020; Shang *et al*., 2014).

3.3.5. Effect of initial metal ion concentration and Adsorption Isotherm

The influence of initial Cr(VI) ion concentration was determined by changing metal ion concentration in the range of 100-1000 mg L-1, while maintaining the rest of parameters fixed as optimized in the preceding experiments. At low metal ion concentration, less concentration of Cr(VI) ions was present in the aqueous system and maximum number of metal ions had the chance to interact with active sites being available for adsorption, encouraging 95% metal uptake at 300 mg L-1. As the metal ion concentration increased there is more number of metal ions in aqueous system competing for available binding sites. As a result, the large number of metal ions remain un-adsorbed because of the exhaustion of active functional sites (Khalil *et al*., 2020; Kokab *et al*., 2021). The % removal efficiency of biochar nanocomposite was reduced from 95% to 39.4% with increase in metal ion concentration from 100-1000 mg L-1 (Fig. 5a). To get deep insight into the nature of sorption system, it is required to conduct the study of equilibrium isotherms. Langmuir model (Singh & Sarma, 2016) proposes that adsorption process takes place on homogenous sites via monolayer adsorption with no interaction between adsorbate-adsorbent molecules.

$$q_e = (q_m \cdot K_l \cdot C_e)/(1 + K_l \cdot C_e)$$

Kl is Langmuir constant (L/mg) associated to the energy of sorption and qm is the maximum adsorption capacity of the adsorbent (mg/g), Ce is the concentration of adsorbate at equilibrium and qe represents the sorption capacity at equilibrium (mg L-1). Freundlich isotherm (Korak *et al*., 2017) addresses heterogeneity of adsorbent surface and obeys multilayer adsorption of adsorbate molecules on adsorbent surface.

$$q_e = K_F \ (C_e^{(1/n_F)})$$

where KF ((mg g-1) (L mg-1)1/n) represents the intensity of sorption and nF is the Freundlich dimensionless constants which measures the deviation of sorption process from linearity.

Redlich-Peterson (R-P) isotherm (Murugesan *et al*., 2013) is a 3 parameter model which delineates the homogenous and heterogeneous behaviors of sorption process by incorporating the features of Langmuir and Freundlich models.

$$q_{(e =)} \ (K_R \cdot C_e)/((1+a \cdot \ ⟦C_e⟧ \ ^g))$$

KR is the R-P constant (L g-1), a is R-P isotherm constant (L mg-1), and g is an exponent

which has value in the range of 0 to 1. Ce is the concentration of adsorbate at equilibrium (mg L-1) and qe is the adsorption capacity at equilibrium (mg g-1). The Langmuir, Freundlich and R-P isotherm models (non-linearized) were fitted to the experimental data. The table (3) lists the isotherm model parameters, which delivers that the Langmuir and R-P isotherm models are in

good agreement with experimental data (Fig. 5b) as compared to Freundlich isotherm model. However, the Langmuir isotherm model holds best for adsorption of Cr(VI) on MRHBC, indicating that Cr(VI) uptake obeys monolayer adsorption via chemisorption on the surface of adsorbent. The results show that under optimal conditions of pH (3.0), temperature (50oC), adsorbent dosage of 0.1 g and contact time of 60 min at baseline metal concentration of (100-1000) mg L-1, the maximum Langmuir sorption capacity (qm) of MRHBC for Cr(VI) was 232.75 mg g-1. It can be seen from Table (1) that MRHBC exhibited enhanced adsorption capacity for Cr(VI) than most of the adsorbents reported in the earlier studies.

4. Conclusion

In this study, the use of MRHBC for adsorption of Cr(VI) was explored and batch experiments were conducted for optimizing the sorption process parameters. Superior adsorption (95%) of Cr(VI) was occurred by using MRHBC under acidic pH (3.0) contact time of 60 min, temperature (50oC) and adsorbent dose of 0.1 g. Various adsorption and kinetic models were applied to experimental data, and the fitting results demonstrated that the adsorption agrees well with general-order kinetics and Langmuir adsorption model. The results suggested that MRHBC can scavenge Cr(VI) in less time with appreciable adsorption capacity (232.75 mg g-1). Conflict of Interest; The authors declare no conflict of interest.

Table (1): Comparison of Cr(VI) adsorption potential of various adsorbents

Adsorbent	Adsorption Capacity (mg g^{-1})	References
Rice husk biochar	161.29	(Mohadi et al., 2021)
Walnut shell biochar	94.50	(Kokab et al., 2021)
Sulphuric acid activated rice husk biochar	4.54	(Sarkar et al., 2019)
Cobalt doped biochar	45.45	(Y. Wang et al., 2012)
Iron chloride modified wheat straw biochar	33.41	(Jiang et al., 2022)
Powdered activated carbon	47	(Jung et al., 2013)
Manganese dioxide functionalized exfoliated graphite	0.30	(Jin et al., 2013)
Nitrogen modified peanut hull biochar microspheres	181.82	(Jiahao & Weiquan, 2020)
Zinc chloride activated sea buckthorn biochar	19.30	(Guo et al., 2021)
20% zinc chloride modified cassava sludge biochar	8.44	(J. Yang et al., 2018)

Zinc chloride functionalized acid vinegar residue biochar	9.96	(Ding et al., 2021)
Nitrogen impregnated *loofah* sponge porous biochar	285.71	(F. Chen et al., 2022)
Surface modified magnesium oxide loaded sugarcane biochar	62.30	(Xiao et al., 2018)
Iron/copper loaded *astragalus membranaceus* biochar	100.33	(Shao et al., 2019)
Typha Orientalis C. Presl biochar supported manganese/iron oxide nanoparticles	59.81	(B. Wang et al., 2020)
Manganese sulfide doped corn straw biochar	98.15	(S. Zhang et al., 2019)
Magnetic pinewood biochar	42.70	(P. Yang et al., 2017)
Melamine functionalized bamboo waste biochar	95.30	(Shang et al., 2014)
Urea functionalized bamboo waste biochar	94.20	(Shang et al., 2014)
Iron-zinc ferrate decorated *Macadamia* nutshell biochar	13.90-31.22	(Qhubu et al., 2021)
Mulberry stem derived biochar supported iron/manganese bimetallic oxide composite	56.18	(S. Xu et al., 2021)
Nano zerovalent iron loaded wetland reed biochar	58.28	(Zhu et al., 2018)
Zinc/iron doped acid activated corn stalk biochar	138.89	(Yu et al., 2020)
Manganese/Cobalt hydrous oxide nanoparticles doped rice husk biochar (MRHBC)	232.75	Present study

Table (2): Adsorption kinetics model fitting parameters

Model	Parameter	Value (Cr(VI))
Pseudo-second-order	k_3 (min^{-1})	1.4603 x10^{-4}
	R_{adj}^2	0.9921
	Reduced chi-square	7.9857
	$q_{e,cal}$ (mg g^{-1})	185.784
General	k_3 (min^{-1})	0.04883
Order	R_{adj}^2	0.99725
	Reduced chi-square	2.77989
	$q_{e,cal}$	133.795
	R_{adj}^2	0.9809
Elovich	*Reduced chi-square*	19.31273
	a (mg g^{-1} min^{-1})	6.2383
	b (g mg^{-1})	0.0179

Table (3): Adsorption isotherm model fitting parameters

Model	Parameter	Value (Cr(VI))
Langmuir	K_l (L mg^{-1})	0.00544
	q_m (mg g^{-1})	232.7497
	R_{adj}^2	0.99878
	Reduced chi-square	0.3985
Freundlich	K_F (mg g^{-1} (mg $L^{-1})^{-1/nF}$)	36.1432
	n_F	4.04496
	R_{adj}^2	0.9758
	Reduced chi-square	7.8863
Redlich-Peterson	q_m (mg g^{-1})	374.738
	K_R (L g^{-1})	1.18112
g		1.02473
	a (L mg^{-1})	0.00423
	R_{adj}^2	0.99876
	Reduced chi-square	0.40662

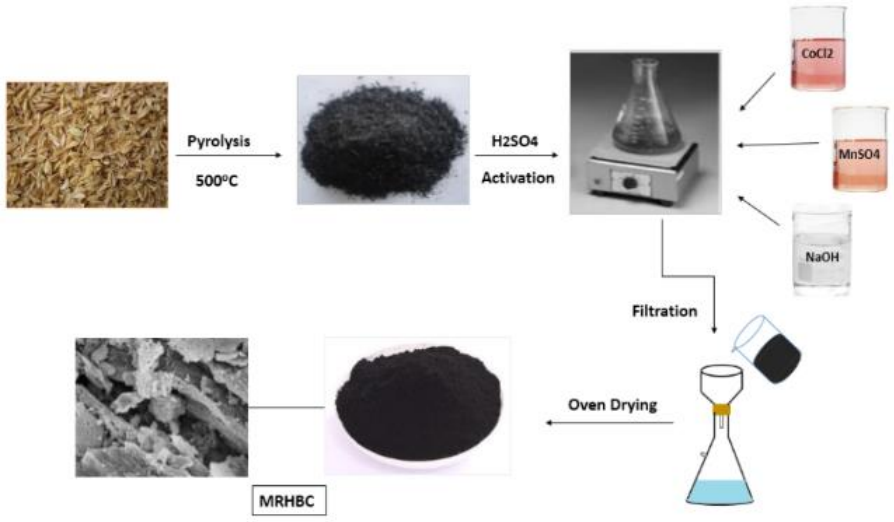

Fig. 1. Schematic illustration of MRHBC fabrication

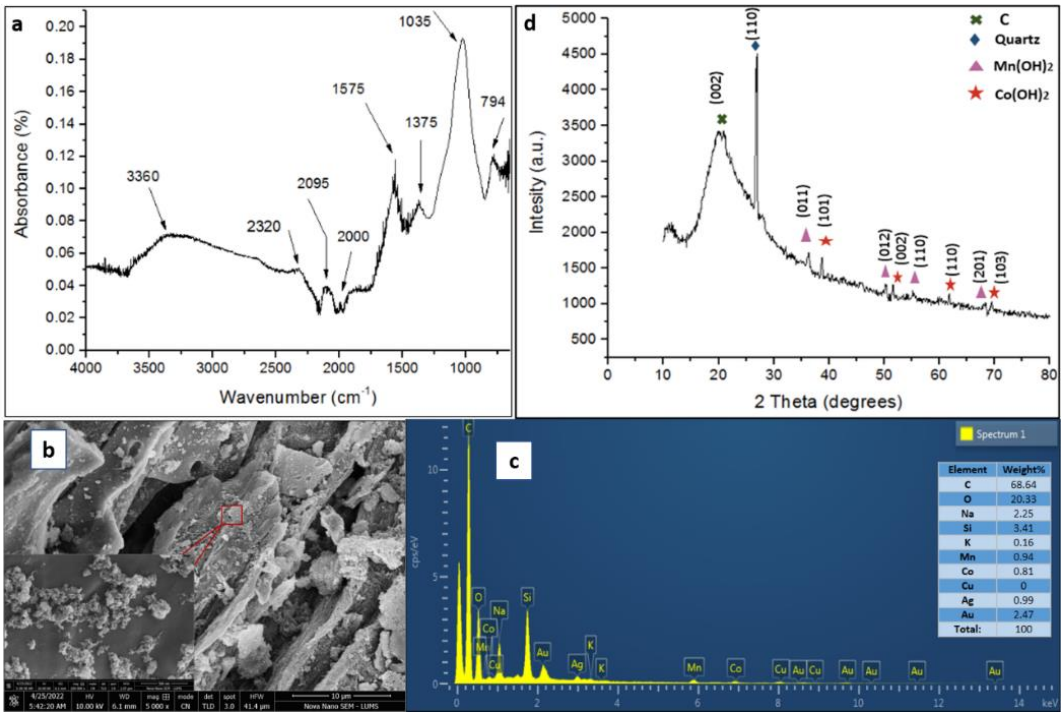

Fig. 2. a) FTIR, b) SEM micrograph c) EDX and d) XRD diffractogram of MRHBC

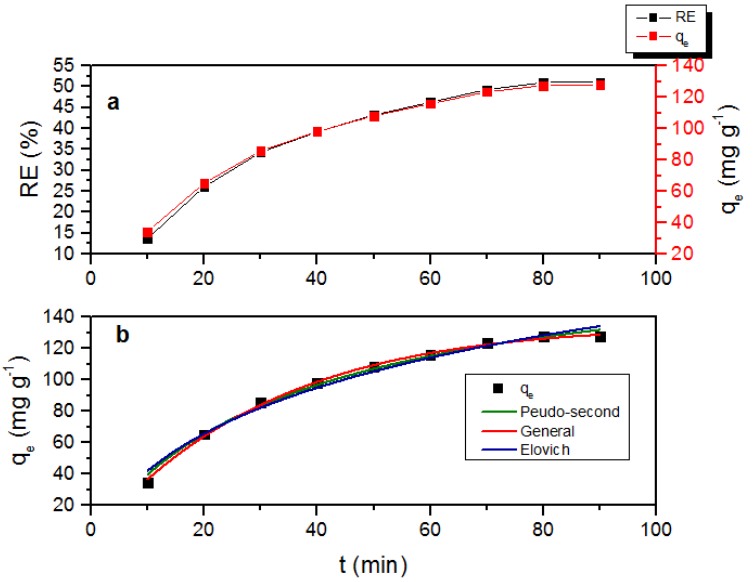

Fig. 3. Effect of variation of time to MRHBC for Cr(VI) adsorption (a), Fitting of kinetic models to MRHBC for adsorption of Cr(VI) (b)

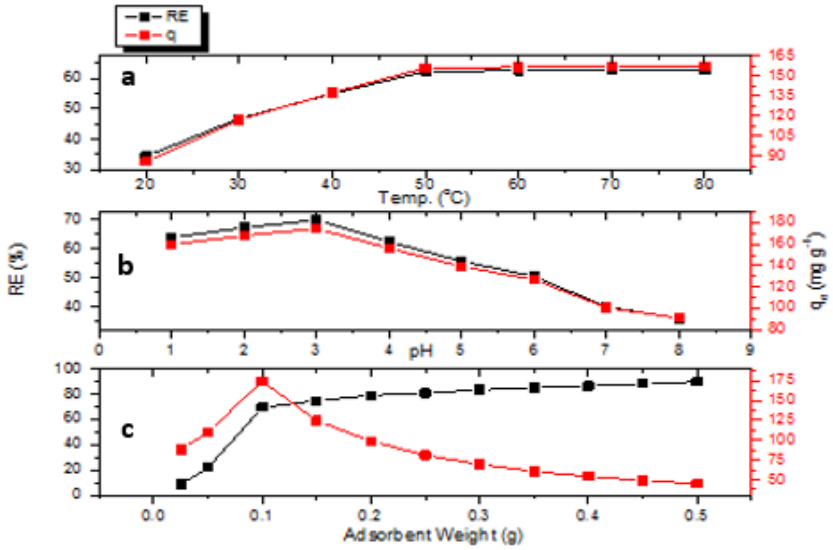

Fig. 4. Effect of variation of temperature (a), pH (b), adsorbent weight (c) on adsorption of Cr(VI)

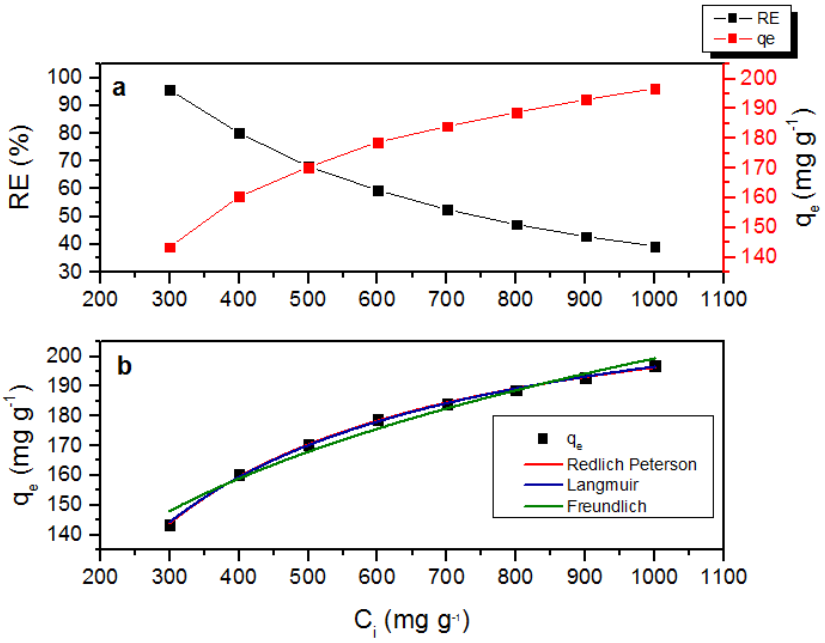

Fig. 5. Effect of variation of initial metal concentration to MRHBC for adsorption of Cr(VI) (a), Fitting of isotherm models to MRHBC for adsorption of Cr(VI)

References

Abyaneh, A. S., & Fazaelipoor, M. H. (2016). Evaluation of rhamnolipid (RL) as a biosurfactant for the removal of chromium from aqueous solutions by precipitate flotation. *Journal of Environmental Management*, 165, 184-187.

Aguilar, C., García, R., Soto-Garrido, G., & Arriagada, R. (2003). Catalytic wet air oxidation of aqueous ammonia with activated carbon. Applied Catalysis B: Environmental, 46(2), 229-237.

Boparai, H. K., Joseph, M., & O'Carroll, D. M. (2011). Kinetics and thermodynamics of cadmium ion removal by adsorption onto nano zerovalent iron particles. Journal of Hazardous Materials, 186(1), 458-465.

Chen, F., Guo, S., Wang, Y., Ma, L., Li, B., Song, Z., . . . Engineering. (2022). Concurrent adsorption and reduction of chromium (VI) to chromium (III) using nitrogen-doped porous carbon adsorbent derived from loofah sponge. 16(5), 1-11.

Chen, T., Liu, R., & Scott, N. R. (2016). Characterization of energy carriers obtained from the pyrolysis of white ash, switchgrass and corn stover—Biochar, syngas and bio-oil. Fuel Processing Technology, 142, 124-134.

Costa, M. (2003). Potential hazards of hexavalent chromate in our drinking water. Toxicology and applied pharmacology, 188(1), 1-5.

Ding, K., Zhou, X., Hadiatullah, H., Lu, Y., Zhao, G., Jia, S., . . . Yao, Y. J. J. o. H. M. (2021).

Removal performance and mechanisms of toxic hexavalent chromium (Cr (VI)) with ZnCl2 enhanced acidic vinegar residue biochar. 420, 126551.

Fraser, B., Pritzker, M., & Legge, R. (1994). Development of liquid membrane pertraction for the removal and recovery of chromium from aqueous effluents. Separation science and technology, 29(16), 2097-2116.

Garcia, X., & Pargament, D. (2015). Reusing wastewater to cope with water scarcity: Economic, social and environmental considerations for decision-making. Resources, Conservation and Recycling, 101, 154-166.

Guo, N., Lv, X., Yang, Q., Xu, X., & Song, H. J. J. o. M. L. (2021). Effective removal of hexavalent chromium from aqueous solution by ZnCl2 modified biochar: effects and response sequence of the functional groups. 334, 116149.

Habiba, U., Siddique, T. A., Joo, T. C., Salleh, A., Ang, B. C., & Afifi, A. M. (2017). Synthesis of chitosan/polyvinyl alcohol/zeolite composite for removal of methyl orange, Congo red and chromium (VI) by flocculation/adsorption. Carbohydrate polymers, 157, 1568-1576.

Ho, Y.-S., & McKay, G. (2002). Application of kinetic models to the sorption of copper (II) on to peat. Adsorption Science & Technology, 20(8), 797-815.

Jiahao, W., & Weiquan, C. J. J. o. E. C. E. (2020). One-step hydrothermal preparation of N-doped carbon spheres from peanut hull for efficient removal of Cr (VI). 8(6), 104449.

Jiang, Y., Dai, M., Yang, F., Ali, I., Naz, I., & Peng, C. J. W. (2022). Remediation of Chromium (VI) from Groundwater by Metal-Based Biochar under Anaerobic Conditions. 14(6), 894.

Jin, H., Yuan, J., Hao, H., Ji, Z., Liu, M., & Hou, S. J. M. l. (2013). The exploration of a new adsorbent as MnO2 modified expanded graphite. 110, 69-72.

Jung, C., Heo, J., Han, J., Her, N., Lee, S.-J., Oh, J., . . . Technology, P. (2013). Hexavalent chromium removal by various adsorbents: powdered activated carbon, chitosan, and single/multi-walled carbon nanotubes. 106, 63-71.

Kamran, U., & Park, S.-J. (2020). MnO2-decorated biochar composites of coconut shell and rice husk: an efficient lithium ions adsorption-desorption performance in aqueous media. Chemosphere, 260, 127500.

Katz, S. A., & Salem, H. (1994). The biological and environmental chemistry of chromium: VCH Publishers.

Kaya, A., Onac, C., & Alpoguz, H. K. (2016). A novel electro-driven membrane for removal of chromium ions using polymer inclusion membrane under constant DC electric current. Journal of Hazardous Materials, 317, 1-7.

Khalil, U., Shakoor, M. B., Ali, S., Rizwan, M., Alyemeni, M. N., & Wijaya, L. J. J. o. S. C. S. (2020). Adsorption-reduction performance of tea waste and rice husk biochars for Cr (VI) elimination from wastewater. 24(11), 799-810.

Kokab, T., Ashraf, H. S., Shakoor, M. B., Jilani, A., Ahmad, S. R., Majid, M., . . . health, p. (2021). Effective removal of Cr (Vi) from wastewater using biochar derived from walnut shell. 18(18), 9670.

Korak, J. A., Huggins, R., & Arias-Paic, M. (2017). Regeneration of pilot-scale ion exchange columns for hexavalent chromium removal. Water research, 118, 141-151.

Lin, J., & Wang, L. (2009). Comparison between linear and non-linear forms of pseudo-first-order and pseudo-second-order adsorption kinetic models for the removal of methylene blue by activated carbon. Frontiers of Environmental Science & Engineering in China, 3(3), 320-324.

Liu, X.-J., Li, M.-F., & Singh, S. K. (2021). Manganese-modified lignin biochar as adsorbent for removal of methylene blue. *Journal of Materials Research and Technology,* 12, 1434-1445.

Mirani, A. A., Kalwar, S., & Ahmad, M. (2013). A rice husk gasifier for paddy drying. *Science Technology and Development (Islamabad),* 32(2), 120-125.

Mishra, S., & Bharagava, R. N. (2016). Toxic and genotoxic effects of hexavalent chromium in environment and its bioremediation strategies. *Journal of Environmental Science and Health, Part C,* 34(1), 1-32.

Mohadi, R., Palapa, N. R., Taher, T., Siregar, P. M. S. B. N., Juleanti, N., Wijaya, A., . . . Technology. (2021). Removal of Cr (VI) from aqueous solution by biochar derived from rice husk. 6(1), 11-17.

Mohamed, A. K., & Mahmoud, M. E. (2020). Nanoscale Pisum sativum pods biochar encapsulated starch hydrogel: a novel nanosorbent for efficient chromium (VI) ions and naproxen drug removal. Bioresource technology, 308, 123263.

Mohan, D., Abhishek, K., Sarswat, A., Patel, M., Singh, P., & Pittman, C. U. (2018). Biochar production and applications in soil fertility and carbon sequestration–a sustainable solution to crop-residue burning in India. RSC advances, 8(1), 508-520.

Mosa, A., El-Ghamry, A., Trüby, P., Omar, M., Gao, B., Elnaggar, A., & Li, Y. (2016). Chemo-mechanical modification of cottonwood for Pb2+ removal from aqueous solutions: Sorption mechanisms and potential application as biofilter in drip-irrigation. Chemosphere, 161, 1-9.

Murugesan, A., Vidhyadevi, T., Kirupha, S. D., Ravikumar, L., Sivanesan, S. J. E. P., & Energy, S. (2013). Removal of chromium (VI) from aqueous solution using chemically modified corncorb-activated

carbon: Equilibrium and kinetic studies. 32(3), 673-680.

Nickens, K. P., Patierno, S. R., & Ceryak, S. (2010). Chromium genotoxicity: a double-edged sword. Chemico-biological interactions, 188(2), 276-288.

Polowczyk, I., Urbano, B. F., Rivas, B. L., Bryjak, M., & Kabay, N. (2016). Equilibrium and kinetic study ofchromium sorption on resins with quaternary ammonium and N-methyl-D-glucamine groups. *Chemical Engineering Journal*, 284, 395-404.

Qhubu, M. C., Methula, B., Xaba, T., Moyo, M., & Pakade, V. E. J. C. A. (2021). Iron-Zinc Impregnated Biochar Composite as a Promising Adsorbent for Toxic Hexavalent Chromium Remediation: Kinetics, Isotherms and Thermodynamics. 1-11.

Qiao, K., Tian, W., Bai, J., Zhao, J., Du, Z., Song, T., . . . Xie, W. (2020). Synthesis of floatable magnetic iron/biochar beads for the removal of chromium from aqueous solutions. *Environmental Technology & Innovation*, 19, 100907.

Sarkar, A., Ranjan, A., Paul, B. J. C. T., & Policy, E. (2019). Synthesis, characterization and application of surface-modified biochar synthesized from rice husk, an agro-industrial waste for the removal of hexavalent chromium from drinking water at near-neutral pH. 21(2), 447-462.

Saucier, C., Adebayo, M. A., Lima, E. C., Cataluña, R., Thue, P. S., Prola, L. D., . . . Dotto, G. (2015). Microwave-assisted activated carbon from cocoa shell as adsorbent for removal of sodium diclofenac and nimesulide from aqueous effluents. *Journal of Hazardous Materials*, 289, 18-27.

Shang, T. X., Zhang, J., Jin, X. J., & Gao, J. M. J. J. o. w. s. (2014). Study of Cr (VI) adsorption onto nitrogen-containing activated carbon preparation from bamboo processing residues. 60(3), 215-224.

Shao, F., Zhou, S., Xu, J., Du, Q., Chen, J., & Shang, J. J. D. W. T. (2019). Detoxification of Cr (VI) using biochar-supported Cu/Fe bimetallic nanoparticles. 158, 121-129.

Shokrani-Havigh, R., & Azizian-Kalandaragh, Y. (2017). Preparation of cobalt hydroxide and cobalt oxide nanostructures using ultrasonic waves and investigation of their optical and structural properties. Journal of Optoelectronics and Advanced Materials, 19(March-April 2017), 283-288.

Singh, K., & Sarma, K. (2016). A simple and feasible approach to decorating MWCNT with Fe3O4 and ZnS and their use as a magnetically separable photocatalyst in the degradation of Cr (VI) in wastewater. Environmental Nanotechnology, Monitoring & Management, 6, 206-213.

Wang, B., Li, F., Wang, L. J. C., & Ecology. (2020). Enhanced hexavalent chromium (Cr (VI)) removal from aqueous solution by Fe–Mn oxide-modified cattail biochar: adsorption characteristics and mechanism. 36(2), 138-154.

Wang, X. S., Chen, L. F., Li, F. Y., Chen, K. L., Wan, W. Y., & Tang, Y. J. (2010). Removal of Cr (VI) with wheat-residue derived black carbon: reaction mechanism and adsorption performance. Journal of Hazardous Materials, 175(1-3), 816-822.

Wang, Y., Wang, X., Liu, M., Wang, X., Wu, Z., Yang, L., . . . Products. (2012). Cr (VI) removal from water using cobalt-coated bamboo charcoal prepared with microwave heating. 39, 81-88.

Xiao, R., Wang, J. J., Li, R., Park, J., Meng, Y., Zhou, B., . . . Zhang, Z. J. C. (2018). Enhanced sorption of hexavalent chromium [Cr (VI)] from aqueous solutions by diluted sulfuric acid-assisted MgO-coated biochar composite. 208, 408-416.

Xiao, R., Wang, S., Li, R., Wang, J. J., & Zhang, Z. (2017). Soil heavy metal contamination and health risks associated with artisanal gold mining in Tongguan, Shaanxi, China. Ecotoxicology and environmental safety, 141, 17-24.

Xu, S., Liang, M., Ding, Y., Wang, D., Zhu, Y., & Han, L. J. F. i. E. C. (2021). Synthesis, optical characterization, and adsorption of novel hexavalent chromium and total chromium sorbent: a fabrication of mulberry stem biochar/Mn-Fe binary oxide composite via response surface methodology. 2, 692810.

Xu, X., Hu, X., Ding, Z., & Chen, Y. (2017). Effects of copyrolysis of sludge with calcium carbonate and calcium hydrogen phosphate on chemical stability of carbon and release of toxic elements in the resultant biochars. Chemosphere, 189, 76-85.

Yang, J., Li, C., Yang, B., Kang, S., & Zhang, Z. (2018). Study on adsorption of chromium (VI) by activated carbon from cassava sludge. Paper presented at the IOP conference series: earth and environmental science.

Yang, P., Guo, D., Chen, Z., Cui, B., Xiao, B., Liu, S., . . . technology. (2017). Removal of Cr (VI) from aqueous solution using magnetic biochar synthesized by a single step method. 38(11), 1665-1674.

Yu, Y., An, Q., Jin, L., Luo, N., Li, Z., & Jiang, J. J. B. T. (2020). Unraveling sorption of Cr (VI) from aqueous solution by FeCl3 and ZnCl2-modified corn stalks biochar: Implicit mechanism and application. 297, 122466.

Zhang, M.-m., Liu, Y.-g., Li, T.-t., Xu, W.-h., Zheng, B.-h., Tan, X.-f., . . . Wang, S.-f. (2015). Chitosan modification of magnetic biochar produced from Eichhornia crassipes for enhanced

sorption of Cr (VI) from aqueous solution. RSC advances, 5(58), 46955-46964.

Zhang, S., Zhang, H., Liu, F., Yang, F., Zhou, S., Zheng, K., . . . Ju, M. J. R. a. (2019). Effective removal of Cr (vi) from aqueous solution by biochar supported manganese sulfide. 9(54), 31333-31342.

Zhang, X., Qian, Y., Zhu, Y., & Tang, K. (2014). Synthesis of Mn 2 O 3 nanomaterials with controllable porosity and thickness for enhanced lithium-ion batteries performance. Nanoscale, 6(3), 1725-1731.

Zhang, Y., Liu, N., Yang, Y., Li, J., Wang, S., Lv, J., & Tang, R. (2020). Novel carbothermal synthesis of Fe, N co-doped oak wood biochar (Fe/N-OB) for fast and effective Cr (VI) removal. Colloids and Surfaces A: Physicochemical and Engineering Aspects, 600, 124926.

Zhou, T., Cao, Z., Tai, X., Yu, L., Ouyang, J., Li, Y., & Lu, J. (2022). Hierarchical Co (OH) 2 Dendrite Enriched with Oxygen Vacancies for Promoted Electrocatalytic Oxygen Evolution Reaction. Polymers, 14(8), 1510.

Zhu, S., Huang, X., Wang, D., Wang, L., & Ma, F. J. C. (2018). Enhanced hexavalent chromium removal performance and stabilization by magnetic iron nanoparticles assisted biochar in aqueous solution: mechanisms and application potential. 207, 50-59.